Design of Reaction Wheel Drive based on Gallium Nitride MOSFETs

Abdallah Alansaari, Alexandros Tsoupos, Prashanth Reddy Marpu
Khalifa University of Science, Technology & Research
United Arab Emirates, Abu Dhabi, Masdar Campus; +971552808088
abaalansari5@gmail.com

ABSTRACT

Key characteristics of wide band-gap semiconductor devices are high dielectric strength, high operating temperature, high current density, high switching-speed and low on-resistance. This set of advantages in comparison to conventional Si-based semiconductors render wide band-gap devices considerably attractive, especially in applications that would gain significant benefits from higher efficiencies and smaller sizes. A CubeSat is a typical example where the available power, volume and mass resources are limited and an overall miniaturization of the avionics is required in order to enable the spacecraft to host multiple and more complex payloads. High-speed brushless DC motors such as those used in modern reaction wheel modules require higher inverter switching frequencies than Si-based inverters can achieve, in the range of 40 kHz to 100 kHz, to minimize losses and torque ripple within the motor and/or to avoid electromagnetic interference with other spacecraft sensors and subsystems. In this paper, we present an initial investigation of a high speed drive based on Gallium-Nitride (GaN) mosfets. The future objective of this setup is to drive an integrated miniature high speed Reaction Wheel system. An initial laboratory prototype is developed to test and validate the performance of the drive.

INTRODUCTION

Accurate attitude control is an essential requirement in many modern satellite missions, especially where Earth-imaging is involved. Many factors affect the quality of attitude control, but the maximum torque and momentum capacities of the actuators are the main dictators.[1] For CubeSat applications, fine attitude control can be achieved using reaction wheels.[1,2] The performance of such reaction wheels can be assessed by evaluating the maximum angular momentum, maximum output torque, electrical power, and the level of micro-vibrations generated by the wheels.[2] Due to size limitations of CubeSats, State of the Art of attitude control actuators is based on miniaturizing technology without significant degradation of the overall performance.[2] This paper proposes a way of achieving this requirement by using Gallium-Nitride (GaN) based brushless DC (BLDC) motor drives, instead of the conventional Silicon (Si) based ones, to drive miniaturized reaction wheels.

Modern reaction wheel modules utilize high speed brushless DC motors, which require high inverter switching frequencies in the range of 40 kHz to 100 kHz to minimize losses and torque ripple within the motor, and to avoid electromagnetic interference with other spacecraft sensors and subsystems. Specifically, the phase current ripple is inversely proportional to the pulse width modulation (PWM) switching frequency. The phase current ripple contributes to motor losses, which reduce the efficiency and increase the temperature of the motor. These losses are especially present in motor-integrated low-voltage battery operated power electronics drives such as 12-V or 5-V, where any additional motor losses will limit the maximum power of the device over the rated operating temperature range leading to a requirement of additional heat sinks, which will increase the system this increases system cost, weight, and space.[3]

This problem can be solved using GaN FETs instead of Si FETs. GaN is characterized as a wide band gap semiconductor because of its three times bigger band gap when compared to Si. Wide band-gap semiconductor devices have higher critical electrical field and higher breakdown voltage for the same material thickness, when compared to Si devices, resulting in significantly smaller channel lengths and on-state resistance, leading to smaller conduction losses. Moreover, when compared to Si devices, GaN devices have smaller gate source and drain source capacitances allowing faster switching with lower switching losses, making them an ideal choice for high switching frequency applications.[4]

In this work, a comparison between GaN BLDC motor drive and Si BLDC motor drive was made. Both drives have similar power ratings and driving the same load. Moreover, both drives were fed the same PWM signal, which is the output of a controller operating with Field Oriented Control (FOC) algorithm.

CONTROL SCHEMES FOR BLDC MOTORS

Trapezoidal control for BLDC

The trapezoidal control scheme is characterized by a two phase ON operation to control the 3-phase inverter.[5] In this scheme only one phase current could be activated at a time, and there should be no torque production in the region of the back EMF zero

crossings. The principle of the trapezoidal scheme is, at all times, to activate the phase pair which can produce the highest torque

The profile of the back EMF of a BLDC motor is of a trapezoidal shape. The back EMF is directly proportional to the motor speed, and the output electromagnetic torque is directly proportional to the phase current. By combining the trapezoidal back EMF with a DC current it makes it possible theoretically to produce a constant torque.[5] However, in practice, the current cannot be initiated instantaneously in a motor phase. Therefore, using this scheme produces a torque ripple at each 60° phase commutation.

Basics of FOC

In general, the basic idea behind FOC is to use a specific coordinate system, where the torque and flux could be controlled independently from each other.[6,7] By choosing a rotating reference frame 'dq', which rotates synchronously with the rotor flux, the rotor flux can be controlled directly by the component of the stator current that is parallel to the rotor flux (the real part of the stator current i_{sd}). By forcing the component of the stator current that is perpendicular to the rotor flux (the imaginary part of the stator current i_{sq}) to be null, the rotor flux orientation is achieved. This corresponds to a first order dynamic system, with a time constant τ_r as given by:

$$\psi_{rd} = \frac{L_m}{\tau_r \cdot s + 1} \cdot i_{sd} \tag{1}$$

where ψ_{rd} = rotor flux; τ_r = time constant = L_r / R_r.

The electromagnetic torque T is proportional to the rotor flux ψ_{rd} and the quadrature component of the stator current i_{sq}. The rotating frame used is synchronous to the rotor flux ψ_{rd}, thus the rotor flux is controlled as a constant by direct stator current i_{sd}. Therefore, the electromagnetic torque T can only be controlled by i_{sq}:

$$T = \frac{3}{2} \cdot \frac{L_m}{L_r} \cdot p \cdot \psi_{rd} \cdot i_{sq} \tag{2}$$

From equations (1) and (2), it can be concluded that both the rotor flux ψ_{rd} and the electromagnetic torque T can be controlled independently from each other. The real and imaginary parts of the stator current (i_{sd} and i_{sq}) commands ψ_{rd} and T respectively.

Implementation of FOC for a Permanent Magnet Brushless DC Motor

For a permanent magnet brushless DC motor, the rotor flux is constant. Another way of representing the electromagnetic torque T is given by the cross product between the stator flux and rotor flux:

$$T = \vec{B}_{stator} \times \vec{B}_{rotor} \tag{3}$$

The maximum torque is obtained when the angle between the stator flux and rotor flux is 90 degrees. Using the "d-q" reference frame, this translates to forcing the real part of the stator current i_{sd} to be zero, and setting the imaginary part of the stator current i_{sq} to be proportional to the desired torque. In theory, by continuously sustaining 90 degrees angle between the stator and rotor flux, the output torque ripple can be driven to zero.

The following steps explains the systematic approach of implementing FOC:[7,8]

Step 1:

Obtain the 3-phase stator currents by measuring two of the phases and calculating the third using the relationship:

$$i_a + i_b + i_c = 0 \tag{4}$$

Step 2:

Convert the 3-phase stator currents into two axis frame "α-β" using Clark's Transformation, which is given by:

$$i_\alpha = i_a \tag{5}$$

$$i_\beta = (i_a + 2i_b) / \sqrt{3} \tag{6}$$

The "α-β" system is on a fixed frame parallel to the stator.

Step 3:

Convert the currents from "α-β" frame to "d-q" frame using Park's transformation given by:

$$i_{sd} = i_\alpha \cos\theta + i_\beta \sin\theta \tag{7}$$

$$i_{sq} = -i_\alpha \sin\theta + i_\beta \cos\theta \tag{8}$$

where θ = rotor flux angle.

Step 4:

Implement two PI controllers to set the value of i_{sd} to zero and the value of i_{sq} to the desired reference value based on the desired torque. The outputs of these controllers are V_{sd} and V_{sq} respectively.

Step 5:

Transform the outputs of the PI controllers, V_{sd} and V_{sq}, back the fixed stator frame "α-β" using Inverse Park's transformation given by:

$$V_\alpha = V_d \cos\theta - V_q \sin\theta \quad (9)$$

$$V_\beta = V_d \sin\theta + V_q \cos\theta \quad (10)$$

Step 6:

Convert the two axis "α-β" voltages into 3-phase voltages using Inverse Clark's transformation given by:

$$V_a = V_\beta \quad (11)$$

$$V_b = (-V_\beta + \sqrt{3}V_\alpha)/2 \quad (12)$$

$$V_c = (-V_\beta - \sqrt{3}V_\alpha)/2 \quad (13)$$

These resulting 3-phase voltage signals are used to generate the PWM signals, which fed into the motor drive. Figure 1 shows the basic scheme of the torque control using FOC.

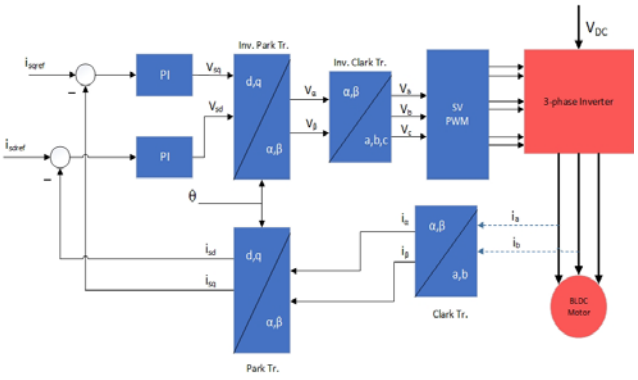

Figure 1: Basic Scheme of FOC

HARDWARE DESCRIPTION

This section covers the main hardware components used in this experiment of comparing between the GaN and Si drives for driving a BLDC motor. The results will be built upon to be later used for driving miniaturized reaction wheels for attitude control of CubeSats. The scope of this experiment is limited to the evaluation of some performance differences between GaN and Si drives BLDC drives.

Brushless DC Motor

The motor used in this experiment is of Anaheim Automation BLY17 Brushless DC motors series.[9] It has high power density with a maximum speed of 4000 rpm. It operates at a rated voltage of 24V and rated current of 7 Amps. It weighs around 0.8kg. Figure 2 shows an illustration of the motor.

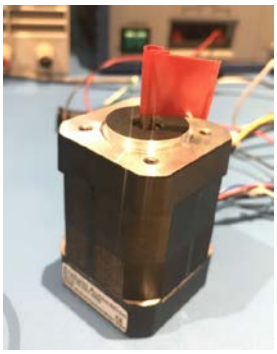

Figure 2: BLDC motor illustration

GaN BLDC Motor Drive

The GaN motor drive used in this experiment is based on Texas Instruments reference design TIDA-00909.[3] The board consists of 3-phase GaN inverter which is capable to drive the motor with switching frequencies up to 100kHz. The GaN FETs have a current rating of 10-A peak current per phase. It operates at nominal voltage of 48V and can go up to 80V providing a maximum output power of 400W. The module has integrated packages where both the GaN FET and its driver is placed in a single package to reduce parasitic inductances and optimize the switching performance to reduce losses, and ultimately help downsize the design and eliminate the heatsink. Figure 3 presents the basic block schematics of the GaN module.[3]

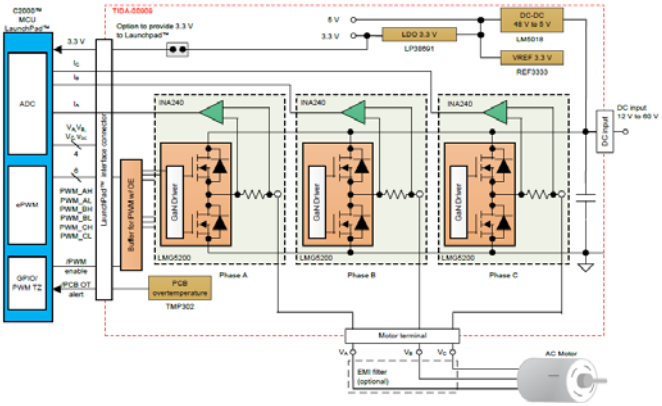

Figure 3: Schematics of GaN motor drive module[3]

Si BLDC Motor Drive

In order to be able to compare between GaN and Si motor drives at a high output switching frequency, Texas Instruments DRV10970 drive was used.[10] This Si drive is able to generate an output PWM signal with a switching frequency of 25kHz. It has integrated FETs that has a peak current rating of 1.5-A per phase. It can accept a range of input voltages between 5V and 18V. It has a built in trapezoidal and sinusoidal commutations used to generate the PWM signals to drive the inverter gates. Figure 4 shows the electric schematics of the Si drive.

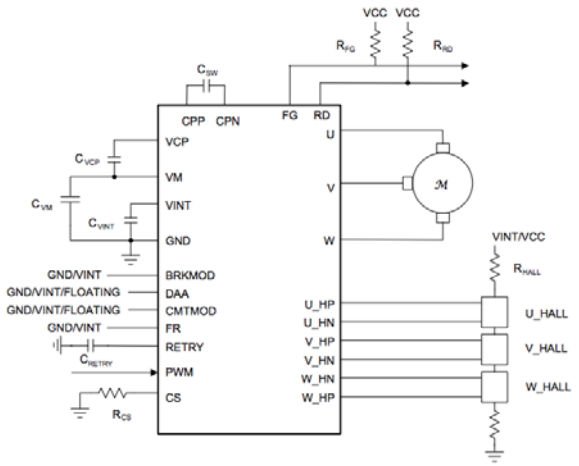

Figure 4: Electric Schematics of the Si Drive[10]

Experimental Setup

Figure 5 illustrates the experimental setup used to perform the comparison between the GaN and Si BLDC motor drives.

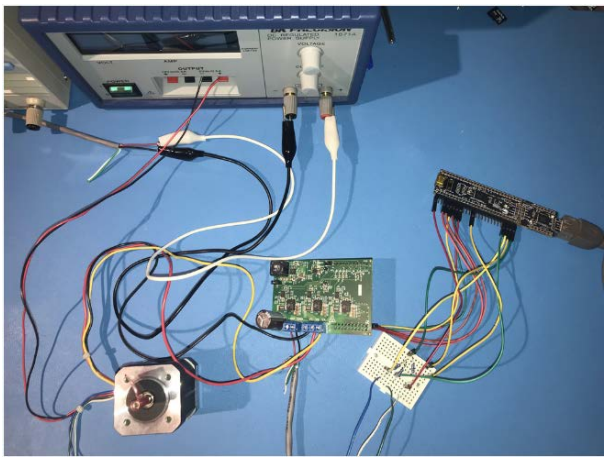

Figure 5: Experimental Setup

RESULTS AND DISCUSSION

Rotor Ripple Speed Test

This section presents the results of the comparisons done between the GaN and Si drives. The first comparison was performed by comparing the speed ripple in the output of the motor. In the following figures the speed was calculated using the rising edge of the hall effect sensors. Figure 6 shows the comparison between the rotor speed ripple of the motor, at different rpms, when driven by the GaN drive, against the motor ripple when driven by Si drive. The output PWM switching frequency was kept constant at 25 kHz, and the DC input to the inverter was kept constant at 15V. The control scheme used in generating the PWM was Trapezoidal control for both drives.

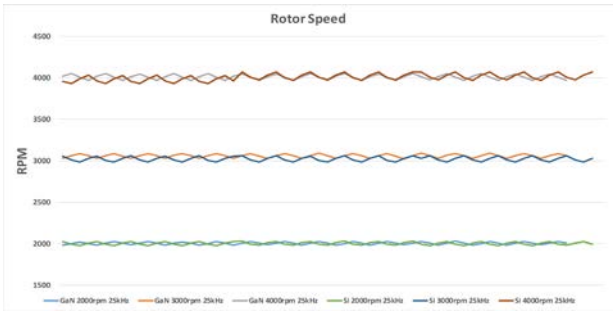

Figure 6: Speed Ripple GaN versus Si (at 25kHz)

In Figure 6, it can be seen that the ripple in the output speed is not zero for both GaN and Si measurements. This is expected since the Trapezoidal control scheme was used to generate the PWM signals.

The PWM output switching frequency was then increased to 100kHz, which is the maximum rating for the GaN drive. Figure 7 shows the comparison in speed ripple for the output of the motor driven by the GaN at 25kHz and 100kHz. Si was excluded from this test because it cannot be driven by frequencies above 25kHz.

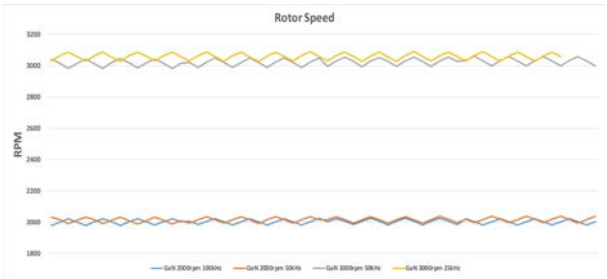

Figure 7: Speed Ripple GaN (25kHz vs 100kHz)

From Figure 7, it can be concluded the switching frequencies at 25kHz and 100kHz produces similar results.

Switching Node Characteristics

The second experiment was related to the switching node characteristics, mainly the turn-on and turn-off times. Figure 8 and 9 shows respectively the turn-on and turn-off waveforms of GaN FETs. On the other hand, Figure 10 and 11 shows respectively the turn-on and turn-off waveforms of SI FETS.

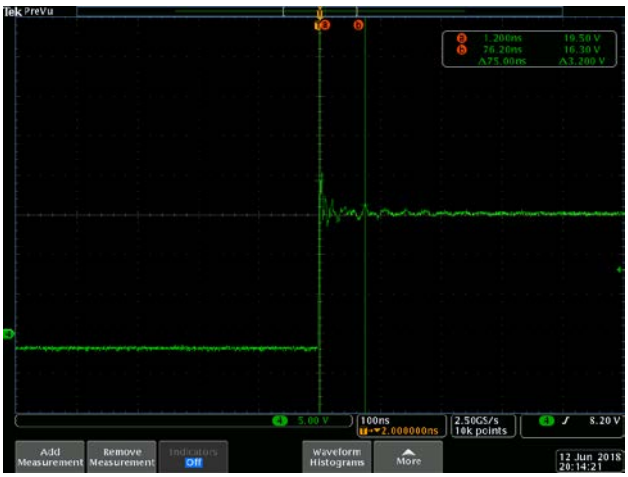

Figure 8: Turn-On Time for GaN FET

Figure 9: Turn-Off Time for GaN FET

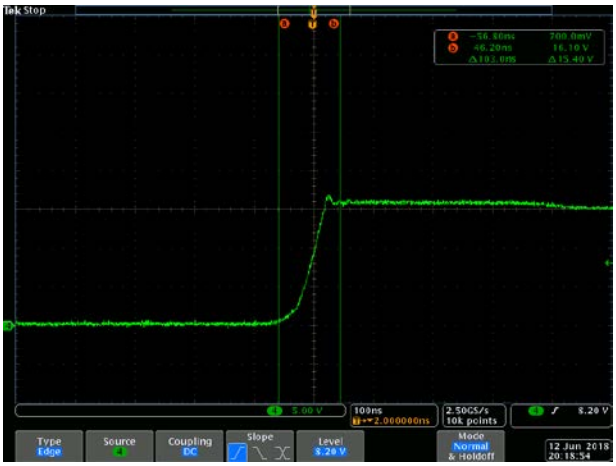

Figure 10: Turn-On Time for Si FET

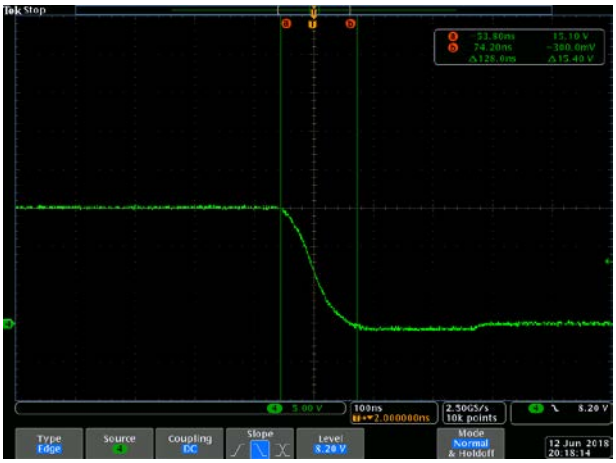

Figure 11: Turn-OFF Time for Si FET

It can be clearly seen that the GaN drive has a faster switching response than Si drive. Comparing Figure 8 and 10, the turn-on time for GaN is lower than that of Si, 75ns versus 103ns respectively. Moreover, as illustrated in figures 9 and 11, the GaN drive surpassed the Si drive with a much lower turn-off time, 55ns versus 128ns respectively. This result is as expected, since GaN is devoid of reverse recovery minority carriers.

These lower switching times corresponds to lower switching losses, which not only makes the system more efficient, but also help in miniaturizing the size of the system since no additional heatsinks are needed.

CONCLUSION AND FUTURE WORK

The wide band-gap characteristics of GaN FETs allow them to have much higher switching frequencies with considerably lower switching losses. GaN drives are very attractive when it comes to driving high speed low voltage BLDC motors. The knowledge learned through the experiments presented in this paper, will help in developing an optimized GaN drive hardware design to drive miniaturized reaction wheels be used by small CubeSats. Furthermore, development of closed loop FOC is going to help in a better quality output with relatively no torque ripple.

REFERENCES

1. Yoon, Hyungjoo, Hyun Ho Seo, and Hong-Taek Choi. "Optimal Uses of Reaction Wheels in the Pyramid Configuration Using a New Minimum Infinity-Norm Solution." *Aerospace Science and Technology* 39 (December 1, 2014): 109–19.
2. Kovo, Yael. "State of the Art Report." NASA, February 20, 2015. http://www.nasa.gov/centers/ames/engineering/state-of-the-art.
3. TI Designs 48-V, 10-A, High-Frequency PWM, 3-Phase GaN Inverter Reference Design for High-Speed Motor Drives
4. Gachovska, T. K., and C. Gerolami. "Comparison of Si and GaN-FETs in a VAR Compensation Application." In *2016 IEEE Electrical Power and Energy Conference (EPEC)*, 1–3, 2016. https://doi.org/10.1109/EPEC.2016.7771747.
5. Akin, Bilal, Manish Bhardwaj, and Jon Warriner. "Trapezoidal Control of BLDC Motors Using Hall Effect Sensors," n.d., 34.
6. Wang, Fengxiang, Zhenbin Zhang, Xuezhu Mei, José Rodríguez, and Ralph Kennel. "Advanced Control Strategies of Induction Machine: Field Oriented Control, Direct Torque Control and Model Predictive Control." Energies 11, no. 1 (January 3, 2018): 120. https://doi.org/10.3390/en11010120.
7. Ramamoorthy, Ramesh T, Brett Larimore, and Manish Bhardwaj. "Sensored Field Oriented Control of 3-Phase Permanent Magnet Synchronous Motors Using TMS320F2837x," 2016, 39.
8. Kumar, B. P., and Krishnan C. M. C. "Comparative Study of Different Control Algorithms on Brushless DC Motors." In *2016 Biennial International Conference on Power and Energy Systems: Towards Sustainable Energy (PESTSE)*, 1–5, 2016. https://doi.org/10.1109/PESTSE.2016.7516444.
9. BLY, The. "BLY17 Series - Brushless DC Motors," n.d., 3.
10. "DRV10970 20W, 12V 3-Phase Sensored BLDC Motor Driver with Single/3halls Supported | TI.Com." Accessed June 13, 2018. http://www.ti.com/product/DRV10970.